Japan J. Indust. Appl. Math. (2013) 30:529–543
DOI 10.1007/s13160-013-0115-3

ORIGINAL PAPER **Area 1**

Local flux conservative numerical methods for the second order elliptic equations

Sunyoung Bu · Won-Tak Hong · June-Yub Lee

Received: 2 December 2012 / Revised: 11 April 2013 / Published online: 18 September 2013

Abstract A discontinuous Galerkin type nonconforming element method and a local flux matching nonconforming element method for the second order elliptic boundary value problems are presented. Both of these methods enjoy the local flux conservation property. The local flux matching method finds a numerical solution in the same solution space of the DG type nonconforming element method, but it achieves much faster iterative convergence speed by embedding continuity requirement in the approximation functions rather than using constraint equations that are used in the DG type nonconforming element method. The merits of the proposed local flux matching method are as follows: the formulation of the method is simple and the solution satisfies local flux conservation property. Moreover, it can be easily applied to general elliptic equations.

Keywords Local flux conservation · Elliptic boundary value problem
Nonconforming element · Finite volume method · GMRES

Mathematics Subject Classification (2000) 65N30 · 65N08 · 65F10

This work was supported by the Priority Research Centers Program (2009-093827) and the Basic Science Research Program (2012-002298) through the National Research Foundation (NRF) of Korea.

S. Bu · W.-T. Hong
Institute of Mathematical Sciences, Ewha Womans University, Seoul 120-750, Korea
e-mail: syboo@ewha.ac.kr

W.-T. Hong
e-mail: wontak@ewha.ac.kr

J.-Y. Lee (✉)
Department of Mathematics, Ewha Womans University, Seoul 120-750, Korea
e-mail: jyllee@ewha.ac.kr

1 Introduction

There are many numerical methods that can be used to solve second order elliptic PDEs—finite element method (FEM), finite volume method (FVM), and boundary element method (BEM) to name a few. Although in most cases there is a way to obtain local flux conservation property, in general, a numerical method may fails to have the local flux conservation property in their most simplest form. The finite element method (FEM) has been developed in its theory and analysis [1,2,5] and has been successful to solve many problems involving complicated domains. Since the classical formulation of FEM does not have local flux conservation property, mixed finite element methods [3,5,15] are developed to properly compute the flux. Finite volume method (FVM) [4,8,9] has been popular because of the local conservation property. FVM is also easy to implement when dual mesh is provided, however, it has some difficulties in designing primal and dual partitions. Recently, the cell boundary element method (CBEM) was introduced by Jeon et al. [10–12]. In CBEM, the average flux on each edge of a cell is evaluated by using the Dirichlet-to-Neumann map and matched along each interface to ensure flux continuity. The CBEM enjoys local conservation property and provides normal flux continuity under certain conditions.

In this paper, we introduce two new flux conservative numerical methods—DG type nonconforming element method and local flux matching method—for a second order general elliptic problem:

$$\begin{aligned} \nabla \cdot (A(x)\nabla u(x)) + V(x) \cdot \nabla u(x) + k(x)u(x) &= f(x) \quad \text{in } \Omega, \\ u(x) &= g(x) \quad \text{on } \Gamma \end{aligned} \tag{1}$$

where $A(x) \in \mathbb{R}^{d\times d}$, $V(x) \in \mathbb{R}^d$, and $k(x) \in \mathbb{R}$. Proposed methods show similarity between FVM and share some of the advantages of FVM: simple to implement, easy to model complex geometry, and most of all, local flux conservation. However, unlike the FVM which is formulated from conservation law, the new methods are derived from matching the average of the primary variable and the flux on each interface. Also, proposed methods are fundamentally different from FEM and nonconforming finite element method [6,13,14] because we are not solving variational equations. In our case, numerical fluxes are matched at each triangular interface without interpolation or penalization or flux limiters. Although our approach might look similar to $p1$-nonconforming FEM, the solution space of our proposed methods contain nonharmonic functions which distinguishes our approach with a $p1$-nonconforming FEM.

Each of the proposed methods has dissimilar numerical representation for the solution and results in different linear systems. Nevertheless, the two proposed methods seek exactly the same mathematical solution. The first (DG type nonconforming element) method, which is easier to understand, will turn out to be inefficient, while the second (local flux matching) method is more efficient than the first one in that the resulting system size is much smaller and the iteration converges much faster.

The paper is organized as follows. In Sect. 2, we describe a general framework for two local flux conservation methods. Then, a DG type nonconforming element method is specified in Sect. 3 and a local flux matching method is described in Sect. 4.

In order to clarify the description, we simply use a Poisson equation $\triangle u = f$ in Ω with Dirichlet boundary condition $u = g$ on Γ in Sects. 2 through 4. The first numerical example in Sect. 5 compares the DG type nonconforming method and the local flux matching method. The second and the third examples present a simple modification of the local flux matching method for a general elliptic BVP in the form of $\nabla \cdot (\epsilon(x)\nabla u(x)) + k(x)u(x) = f(x)$ and numerical computations show that the method has the optimal order of convergence in H^1-norm and L^2-norm. Concluding remarks are given in Sect. 6.

2 A local flux conservative numerical scheme

For clarity, we restrict our discussion to the Poisson equation on a convex domain $\Omega \in \mathbb{R}^2$ with a smooth boundary $\Gamma = \partial\Omega$ with Dirichlet boundary conditions,

$$\begin{aligned} \Delta u &= f \text{ in } \Omega, \\ u &= g \text{ on } \Gamma. \end{aligned} \tag{2}$$

Let $\mathcal{T}_h = \{T_1, T_2, \ldots, T_{N_T}\}$ be a triangulation of Ω where N_T is the total number of triangles. We further assume $\mathcal{T}_h$ satisfies $\max_{T_i \in \mathcal{T}_h} d(T_i)/\rho(T_i) \leq C$, where $d(T_i)$ and $\rho(T_i)$ is the diameter of T_i and diameter of inscribed circle in T_i, respectively.

We also denote the total edge set $\mathcal{E}$ as a union of interface set $\mathcal{E}_I = \{E_j\}_{j=1}^{N_I}$ and boundary set $\mathcal{E}_B = \{E_{j+N_I}\}_{j=1}^{N_B}$ where total number of edges N_E is $N_I + N_B$. Furthermore, we denote $i^+(j)$ and $i^-(j)$ for indices of outer and inner adjacent triangles for each interface $E_j \in \mathcal{E}_I$, respectively.

We define the approximation space V with first order polynomials V^L and non-harmonic functions V^F as follows

$$V = V^L \oplus V^F \tag{3}$$

where

$$V^L := \{v_i \mid v_i \in P_1(T_i),\ i = 1, 2, \ldots, N_T\}, \tag{4}$$

$$V^F := \{F_i \mid \text{supp}(F_i) = T_i,\ i = 1, 2, \ldots, N_T\}. \tag{5}$$

Here, V^L and V^F give the harmonic and non-harmonic part of the approximation function when restricted on a triangle. Note that for each $T_i \in \mathcal{T}_h$, we can decompose a numerical solution

$$v_i(x, y) = a_i + b_i(x_i - \overline{x_i}) + c_i(y_i - \overline{y_i}) + d_i F_i(x, y) \quad \text{for } (x, y) \in T_i \tag{6}$$

into two parts; a non-harmonic function $F_i(x, y) \in V^F$ and the first order polynomial $v_i^L(x, y) = a_i + b_i(x_i - \overline{x_i}) + c_i(y_i - \overline{y_i}) \in V^L$ where $(\overline{x_i}, \overline{y_i})$ is the incenter of T_i.

Our proposed scheme can be summarized in one sentence: Find approximation $v_i = v_i^L + d_i F_i \in V^L \oplus V^F$ satisfying function value and flux continuity conditions

across an interface E_j with $d_i F_i$ generating the total flux of f in T_i. The algorithm can be explained in three steps as follows.

1. For all $T_i \in \mathcal{T}_h$, the following balance equation which is the conservation form of (2) will determine d_i as follows.

$$\int_{T_i} \Delta v = 0 + d_i \int_{\partial T_i} \nabla F_i \cdot \mathbf{n} = \int_{T_i} f \tag{7}$$

where $\mathbf{n}$ denotes the outer normal direction on ∂T_i. Therefore the coefficient d_i can be determined on each $T_i \in \mathcal{T}_h$ as follows,

$$d_i = \frac{\int_{T_i} f}{\int_{\partial T_i} \nabla F_i \cdot \mathbf{n}}. \tag{8}$$

Note that our approximated solution v will always satisfy the conservation law (7) locally for all $T_i \in \mathcal{T}_h$.

2. For each interface $E_j \in \mathcal{E}_I$ between two adjacent triangles $T_{i^+(j)}$ and $T_{i^-(j)}$ as shown in Fig. 1, we match the average jump of v and $\nabla v \cdot \mathbf{n}$ as follows:

$$\langle v \rangle_{E_j} = 0, \tag{9}$$

$$\left\langle \frac{\partial v}{\partial n} \right\rangle_{E_j} = 0 \tag{10}$$

where $\langle V \rangle_{E_j}$ denotes an average jump across E_j,

$$\langle V \rangle_{E_j} = \frac{1}{|E_j|} \int_{E_j} [V(\mathbf{x})]\, d\mathbf{x} \tag{11}$$

and $[V(\mathbf{x})]$ denotes the jump of V at $\mathbf{x} \in E_j = \overline{T}_{i^+(j)} \cap \overline{T}_{i^-(j)}$,

$$[V(\mathbf{x})] = \lim_{h \to 0^+} V_{i^+(j)}(\mathbf{x} + h\mathbf{n}) - \lim_{h \to 0^+} V_{i^-(j)}(\mathbf{x} - h\mathbf{n}). \tag{12}$$

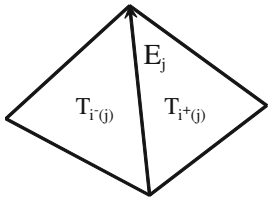

Fig. 1 An interface E_j between two adjacent triangles $T_{i^+(j)}$ and $T_{i^-(j)}$

3. For each Dirichlet boundary segment $E_j \in \mathcal{E}_B$,

$$\int_{E_j} v(\mathbf{x})\, d\mathbf{x} = \int_{E_j} g(\mathbf{x})\, d\mathbf{x}. \tag{13}$$

Before closing the section, we make several comments on this scheme. First, any trial function $v \in V$, V as given in (3), of the proposed scheme will always satisfy the local conservation law on any triangular subregion $D \subset \Omega$. More specifically,

$$\int_D \triangle v(\mathbf{x})\, d\mathbf{x} = \int_{\partial D} \frac{\partial v}{\partial \mathbf{n}} = \sum_{T_i \subset D} \int_{\partial T_i} \frac{\partial v_i}{\partial \mathbf{n}} = \int_D f\, d\mathbf{x}. \tag{14}$$

Second, the resulting non-symmetric system of equations can be effectively solved by GMRES [16] method.

Finally, we emphasize the non-harmonic nature of the F_i in (6) as the most notable feature of our proposed scheme. Of course, one has freedom to choose the space V^F. However, the order of convergence does not seem to depend on the choice of F_i. In this paper we will demonstrate our scheme with two simple examples of F_i.

3 A discontinuous Galerkin type nonconforming element method

We consider a solution of (2) in the form of (6) with a given non-harmonic function $F_i(x, y)$,

$$v_i(x, y) = a_i + b_i(x_i - \overline{x_i}) + c_i(y_i - \overline{y_i}) + d_i F_i(x, y) \tag{15}$$

where d_i can be explicitly computed by (8). There are three unknowns per triangles and total $3N_T$ unknowns, $\{a_i, b_i, c_i\}_{i=1}^{N_T}$. To close $3N_T$ system, we impose the following constraints:

$$\langle v \rangle_{E_j} = 0, \ \left\langle \frac{\partial v}{\partial n} \right\rangle_{E_j} = 0 \tag{16}$$

for each interface E_j, $j = 1, \ldots, N_I$ and

$$\int_{E_j} v(\mathbf{x})\, d\mathbf{x} = \int_{E_j} g(\mathbf{x})\, d\mathbf{x} \tag{17}$$

for each boundary segment E_{N_I+j}, $j = 1, \ldots, N_B$. Here, equation (16) is used to ensure continuity as required by (9) and (10) and Eq. (17) is used to impose boundary condition as given by (13). Therefore, the number of total constraints is $2N_I + N_B$ and it matches exactly with total number of edges in the triangulation which is $3N_T$ because each of the interfaces is counted exactly twice and each of the boundary

segments is counted only once. We call the above $3N_T$-by-$3N_T$ system of equations a DG type "Nonconforming element method" (Method NC). It is well-defined once non-harmonic functions F_i are given.

We consider a solution non-harmonic quadratic polynomial in the replacement of F_i in (15) as follows,

$$v_i(x, y) = a_i + b_i(x_i - \overline{x_i}) + c_i(y_i - \overline{y_i}) + d_i((x_i - \overline{x_i})^2 + (y_i - \overline{y_i})^2) \tag{18}$$

where d_i can be computed by (8), more explicitly as follows,

$$d_i = \frac{\int_{T_i} f(x)}{4|T_i|} = \frac{1}{4}\overline{f_i}. \tag{19}$$

Here $\overline{f_i}$ is the flux preserving piecewise constant approximation of $f_i(x)$ in the triangle. Numerical experiments for the method with non-harmonic quadratic polynomial function (Method $\mathrm{NC_q}$) is given in Sect. 5.

4 A local flux matching nonconforming element method

We introduce a new non-harmonic function $\Lambda_i(x, y)$ to be used for F_i in (15). We specifically design $\Lambda_i(x, y)$ to generate constant flux along all of three edges of T_i. Therefore, with the new non-harmonic function, the numerical solution (6) for the Poisson equation (2) can be written as follows:

$$v_i(x, y) = a_i + b_i(x - \overline{x_i}) + c_i(y - \overline{y_i}) + d_i\Lambda_i(x, y) \tag{20}$$

where the trigonal pyramid shape function $\Lambda_i(x, y)$ is defined in the following paragraph.

For each $T_i \in \mathcal{T}_h$, $\Lambda_i(x, y)$ has a unit height at the incenter of T_i and has 0 values along 3 edges in the triangle. More precisely, we create three sub-triangles by interconnecting two adjacent vertices of the given triangle and the incenter $D_i(\overline{x_i}, \overline{y_i})$ of the triangle T_i as shown Fig. 2.

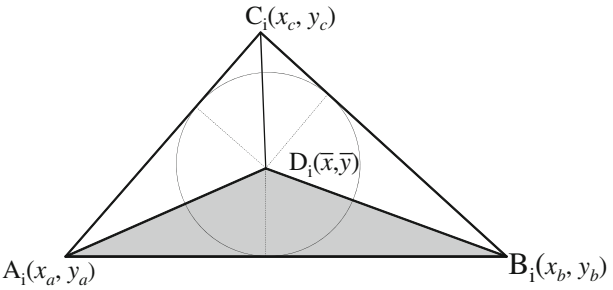

Fig. 2 A triangle T_i and inscribed circle centered at $D_i(\overline{x}, \overline{y})$. Sub-triangle Δ_{ABD} is *shaded*

The piecewise linear function $\Lambda_i(x, y)$ has closed-form representation in each sub-triangles of T_i,

$$\Lambda_i(x, y) = 1 - \frac{(x - \bar{x})(y_b - y_a) - (x_b - x_a)(y - \bar{y})}{(x_a - x_b)(y_b - \bar{y}) - (x_b - \bar{x})(y_a - y_b)}, \quad (x, y) \in \Delta_{ABD} \tag{21}$$

where Δ_{ABD} is one of three sub-triangles of T_i. Similarly, $\Lambda_i(x, y)$ is defined on Δ_{BCD} and Δ_{CAD}. Note that $\Lambda_i(\partial T_i) = 0$ and $\text{supp}(\Lambda_T) = T$.

To find d_i for each triangle T_i, we apply the balance equation (7) on each triangle with the trial function given in (20),

$$d_i \int_{\partial T_i} \frac{\partial \Lambda_i}{\partial \mathbf{n}} = \int_{T_i} f. \tag{22}$$

Note that the normal derivatives of the pyramid shape function Λ_i is constant along the edges in each triangle,

$$\frac{\partial \Lambda_i}{\partial \mathbf{n}} = \frac{1}{\rho_i} \tag{23}$$

where ρ_i is the radius of the inscribing circle in each triangle T_i. Therefore, the coefficient of the non-harmonic term d_i can be obtained using (8),

$$d_i = \overline{f}_i \frac{\rho_i^2}{2} \tag{24}$$

where $\int_{T_i} f = \overline{f_i}\ |T_i|$ and $|T_i| = \frac{1}{2}\rho_i |\partial T_i|$.

Before we proceed to a new local flux matching method, readers can easily see that the coefficient a_i, b_i, and c_i of the solution defined in (15) can be computed if the value d_i is given in similar way as we discussed in previous section, which we refer the method as a nonconforming element method with a pyramid shape function (Method NC_Λ).

Instead of finding unknowns given as coefficients of closed form solution in (20), we set unknowns to function values $v(M_j)$ at the midpoints M_j of all edges $E_j \in \mathcal{E}$. Our element consists of piecewise linear polynomials that are continuous at the midpoint of edges and non-harmonic terms whose boundary values are zero, $\Lambda_i|_{\partial T_i} = 0$. Therefore, continuity at midpoints guarantees average jump condition of v defined in (9), $\langle v \rangle_{E_j} = 0$ and the Dirichlet boundary condition (13) can be set as $v(M_j) = \frac{1}{E_j} \int_{E_j} g(\mathbf{x}) d\mathbf{x}$ for $E_j \in \mathcal{E}_B$ and its midpoint M_j.

To find remaining unknowns $v(M_j)$, $j = 1, \ldots, N_I$, we match local flux continuity condition (10) along the interfaces for $E_j \in \mathcal{E}_I$ as follows:

$$\left\langle \frac{\partial v}{\partial \mathbf{n}} \right\rangle_{E_j} = 0. \tag{25}$$

We name this simple numerical algorithm as "Local flux matching method" (Method LF_Λ). The method LF_Λ finds a solution in the same space as the method NC_Λ with exactly same constraints, however, the number of unknowns N_I is much smaller than $3N_T = 2N_I + N_B$ for NC_Λ. In the essence, the significant saving in the number of unknowns has been possible by introducing the pyramid shape non-harmonic function with zero values along the triangle edges. We will compare numerical properties of these methods in Sect. 5.

5 Numerical results

In this section, we present several numerical results to test performance of the proposed method (LF_Λ) and to compare it with the nonconforming methods (NC_q and NC_Λ). In the first example, we start with a simple Poisson problem and apply all of three methods proposed in Sects. 3 and 4. All of the methods have the same order of convergence, especially NC_Λ and LF_Λ provide exactly same solutions. However, the GMRES convergence speed of the local flux matching method (LF) is much faster than the nonconforming methods (NC). In the second example, we numerically demonstrate that the LF method provides the optimal order of convergence for a variable coefficient conductivity equation $\nabla \cdot (\epsilon(x)\nabla u(x)) = f(x)$. In the third example, we illustrate that it is very easy to modify the LF method for more general type of elliptic equation such as $\nabla \cdot (\epsilon(x)\nabla u(x)) + k(x)u(x) = f(x)$ and the possibility of the proposed LF method as a general tool for wide class of boundary value problems in 2 or 3 dimensional domains.

5.1 Constant coefficient on a nonuniform mesh

First, we consider the following Dirichlet boundary value problems on the unit square domain $\Omega = [0, 1] \times [0, 1]$ with nonuniform mesh seen in Fig. 3,

$$\triangle u = f \quad \text{in } \Omega, \tag{26}$$

$$u = 0 \quad \text{on } \partial\Omega \tag{27}$$

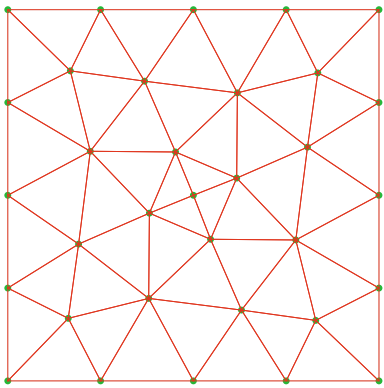

Fig. 3 A nonuniform coarse grid with N_T=48 triangles, N_I=64 interfaces, and N_B=16 boundary edges on the square domain [0, 1] × [0, 1]

where the exact solution is $u(x, y) = \exp^{-(x^2+y^2)} \sin(\pi x) \sin(\pi y)$ and the function f is generated by the exact solution.

In this example, we investigate the convergence order for two different methods (NC and LF) described in Sects. 3 and 4. For the nonconforming (NC) method, we test two different nonharmonic terms (NC_q and NC_Λ).

As described in previous sections, the unknowns of the NC methods are defined for each triangle T_i but those of the LF method are defined on each interface E_j. For the comparison of L^2-error of the NC and the LF methods, we calculate the function value $v_i(D_i)$ at the incenter D_i of each triangle T_i. Relative L^2-error is computed as

$$E_n^2 = \frac{\sum_{i=1}^{N_T} (v_i(D_i) - u(D_i))^2 |T_i|}{\sum_{i=1}^{N_T} (u(D_i))^2 |T_i|}. \tag{28}$$

Relative error in H^1-norm for NC_q is simply calculated as

$$E_n^2 = \frac{\sum_{i=1}^{N_T} (\nabla v_i(D_i) - \nabla u(D_i))^2 |T_i|}{\sum_{i=1}^{N_T} (\nabla u(D_i))^2 |T_i|}. \tag{29}$$

However, we need more complicated calculation for H^1-error for methods (NC_Λ and LF_Λ) since the derivative of the pyramid-shape non-harmonic function Λ is not well-defined at the centroid in each triangle T_i. Therefore, we subdivide a triangle into three smaller triangles with D_i as a new vertex as shown in Fig. 2 and then relative error in H^1-norm is calculated as follows,

$$E_n^2 = \frac{\sum_{i=1}^{N_T} \sum_{K \in \{A,B,C\}} (\nabla v_i(D_i^K) - \nabla u(D_i^K))^2 |T_i^K|}{\sum_{i=1}^{N_T} \sum_{K \in \{A,B,C\}} (\nabla u(D_i^K))^2 |T_i^K|} \tag{30}$$

where D_i^C is a centroid of triangle $T_i^C := \triangle ABD$. D_i^A and D_i^B are those of sub-triangles T_i^A and T_i^B, respectively.

We start with a triangulation having $N_T = 48$ triangles as shown in Fig. 3 and then iteratively subdivide each of triangles in the domain into four equal triangles. Tables 1, 2, and Fig. 4 show relative L^2 and H^1 errors of the numerical computation for $N_T = 48$, $2^2 \cdot 48$, and $2^4 \cdot 48$. Here, the rate of convergence for doubled mesh is calculated as $\alpha = \log_2(E_n / E_{n+1})$.

Note that computed solutions by the method NC_Λ and the method LF_Λ shown in Table 2 are identical since both of them find a solution in the same space $V = V^L \oplus V^F$ with the same constraints even though the linear systems are different. As seen in

Table 1 Relative errors for method (NC_q)

N_T	L^2-norm	α	H^1-norm	α
48	1.5877e−2		1.7459e−1	
192	3.7669e−3	2.0755	8.4818e−2	1.0415
768	9.3229e−3	2.0145	4.2107e−2	1.0103

Table 2 Relative errors for method (NC_Λ) and method (LF_Λ)

N_T	L^2-norm	α	H^1-norm	α
48	2.6413e−2		2.0721e−1	
192	6.4475e−3	2.0344	1.0289e−1	1.0100
768	1.6065e−3	2.0048	5.1380e−2	1.0017

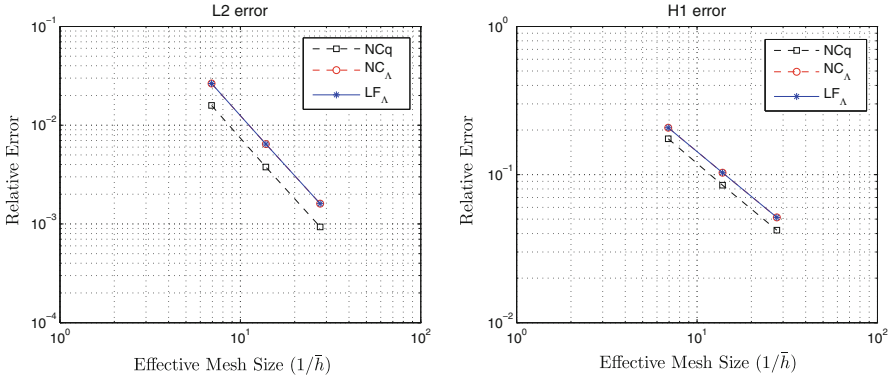

Fig. 4 Order of convergence. L^2 and H^1 relative errors as a function of mesh size are shown. Note that the results for NC_Λ and LF_Λ coincide

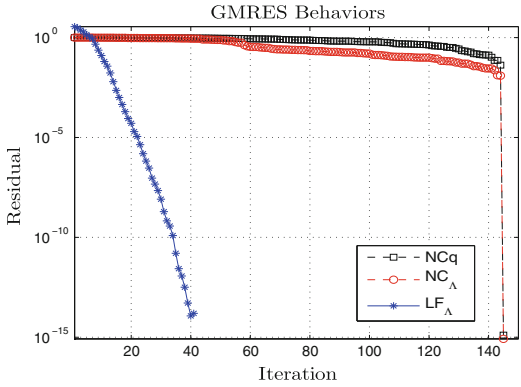

Fig. 5 Iterative convergence behavior of the GMRES method. Linear system size for the method NC_q or NC_Λ is 144×144 and LF_Λ is 64×64

Tables 1 and 2, all of the methods provide the optimal convergence order; 2nd order of convergence in L^2-norm and the 1st order of convergence in the H^1-norm. Figure 4 visualizes the same error data in Tables 1 and 2 as a function of effective mesh size $\bar{h} = \sqrt{|\Omega|/N_T}$.

Even though all of the proposed methods have the same order of convergence, the iterative convergence behavior shows difference (Fig. 5) and is subject to future investigation. Note that the number of unknowns in the LF framework is the number of internal edges N_I while there are $3N_T = 2N_I + N_B$ unknowns in the NC methods, 3 coefficients in each triangle. For example, the system size of the method NC_q or NC_Λ is $3N_T = 144$ and that of LF_Λ is $N_I = 64$ for the triangulation shown in Fig. 3.

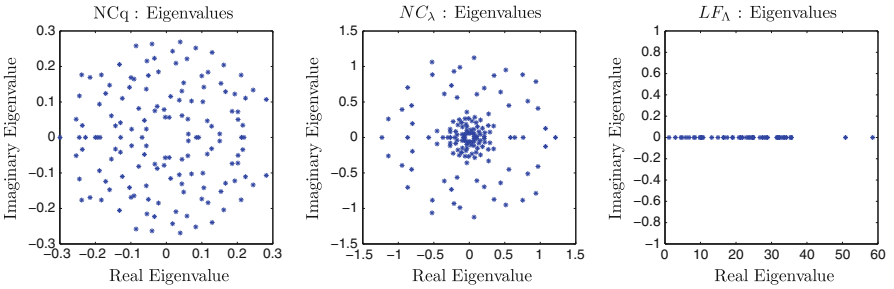

Fig. 6 Distribution of 144 eigenvalues of the method NC_q and NC_Λ and 64 eigenvalues of the method LF_Λ

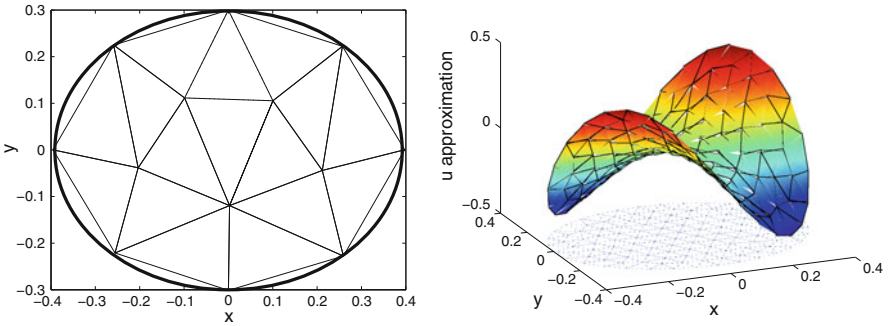

Fig. 7 A coarse mesh on ellipse with $N_T = 16$ triangles and a computed solution on a finer mesh with $N_T = 210$

The convergence speed of the GMRES is determined by distribution of the eigenvalues. Figure 6 shows the eigenvalue distributions of the linear systems for method (NC) and (LF). It explains the numerical experiment in which the LF method is much faster than the NC methods. From this observation, we propose the method LF_Λ as a proper numerical tool to find a solution in the space consisting of the piecewise-linear and non-harmonic functions.

5.2 Variable coefficient problem

In this example, we consider a variable coefficient equation with conductivity $\epsilon(x, y) = 1 + x^2 + y^2$ in the elliptical domain shown in Fig. 7,

$$\nabla \cdot (\epsilon(x, y)\nabla u(x, y)) = f(x, y) \quad \text{in} \quad \Omega, \tag{31}$$

$$u(x, y) = g(x, y) \quad \text{on} \quad \partial\Omega \tag{32}$$

where $f(x, y)$ and $g(x, y)$ are chosen so that the exact solution is $u(x, y) = \exp^{-(x^2+y^2)} \sin(\pi x) \sin(\pi y)$. We slightly modify the LF_Λ method defined in Sect. 4

in order to find a solution in the form of (20) for this kind of variable equations. First, we define a piecewise constant conductivity

$$\bar{\epsilon}(x, y) = \bar{\epsilon}_i \quad \text{for} \quad (x, y) \in T_i \tag{33}$$

where $\bar{\epsilon}_i := \frac{1}{|T_i|} \int_{T_i} \epsilon$. Then d_i defined in (24) should be redefined as

$$d_i = \frac{\overline{f}_i}{\bar{\epsilon}_i} \frac{\rho_i^2}{2}. \tag{34}$$

The resulting system of linear equation for the function value $v(M_j)$ at the midpoint of each interface $\{E_j\}_{j=1}^{N_I}$ comes from the flux continuity equation,

$$\left\langle \bar{\epsilon} \frac{\partial v}{\partial \mathbf{n}} \right\rangle_{E_j} = 0. \tag{35}$$

Figure 7 shows a coarse grid triangulation with $N_T = 16$ and a computational result on a finer grid with $N_T = 210$.

To examine the convergence behavior of the proposed method (LF), we calculate the relative L^2-error and H^1-error. The mean function value on each interface E_j is the computed solution $v(M_j)$ at the midpoint, so it is natural to define a relative L^2-error using these values. The derivative ∇v_i along each side is constant, but the value ∇v is not well-defined on the interface E_j since the tangent derivatives on the left and right triangles are different and the flux across E_j is continuous, $\bar{\epsilon}_{i^+(j)} \frac{\partial v_{i^+(j)}}{\partial \mathbf{n}} = \bar{\epsilon}_{i^-(j)} \frac{\partial v_{i^-(j)}}{\partial \mathbf{n}}$ for two adjacent triangles $T_{i^+(j)}$ and $T_{i^-(j)}$. Therefore, we define a relative H^*-error using continuous normal flux as follows,

$$E_n^2 = \frac{\sum_{j=1}^{N_I} \left(\bar{\epsilon}_{i^+(j)} \frac{\partial v_{i^+(j)}}{\partial \mathbf{n}}(M_j) - \epsilon(M_j) \frac{\partial u}{\partial \mathbf{n}}(M_j) \right)^2}{\sum_{j=1}^{N_I} \left(\epsilon(M_j) \frac{\partial u}{\partial \mathbf{n}}(M_j) \right)^2}. \tag{36}$$

As shown in Fig. 8, numerical results of the proposed method (LF) with $N_T = 16$ to $N_T = 3024$ triangles show the expected optimal second order convergence in L^2-norm sense. The order of convergence in the new H^*-norm is higher than the first order expected for H^1-norm since only normal component $\partial v / \partial \mathbf{n}$ is used instead of the gradient ∇v.

5.3 Helmholtz equations

Our final example is the Helmholtz equations with $\epsilon(x, y) = 1 + x^2 + y^2$ and $k = 1$ on the punctured elliptical domain shown in Fig. 9,

$$\nabla \cdot (\epsilon(x, y) \nabla u(x, y)) + k u = f(x, y) \quad \text{in} \quad \Omega, \tag{37}$$

$$u(x, y) = g(x, y) \quad \text{on} \quad \partial\Omega \tag{38}$$

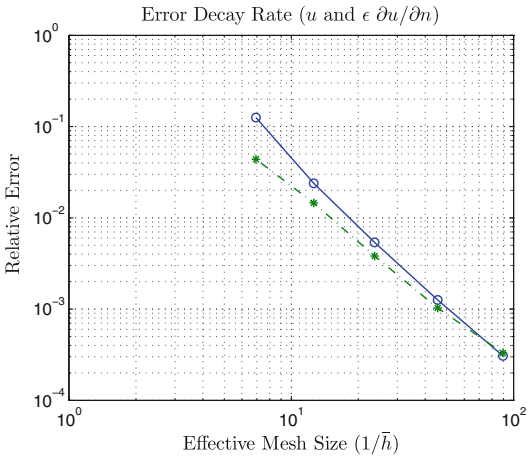

Fig. 8 Decay rates of L^2-error (*solid line*) and H^*-error (*dash-dotted line*) as a function of effective mesh size $\bar{h} = \sqrt{|\Omega|/N_T}$

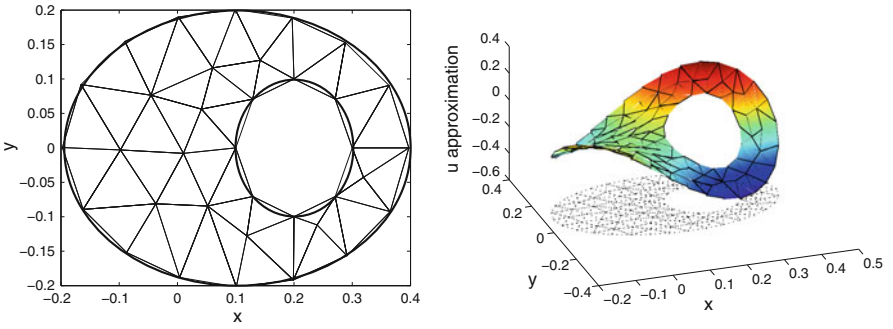

Fig. 9 A coarse mesh on ellipse with $N_T = 46$ triangles and a computed solution on a finer mesh with $N_T = 170$

where $f(x, y)$ and $g(x, y)$ are chosen so that the analytical solution becomes $u(x, y) = \exp^{-(x^2+y^2)} \sin(\pi x) \sin(\pi y)$.

We approximate $\epsilon(x, y)$ by a piecewise constant function $\bar{\epsilon}(x, y)$ as in (33), however, d_i in the solution form (20) can not be directly computed as in (34) since non-harmonic source comes not only from f but also ku. Therefore, we form a linear system with $N_I + N_T$ unknowns, $\{v(M_j)\}_{j=1}^{N_I}$ and $\{d_i\}_{i=1}^{N_T}$. The corresponding constraints equations are

$$\left\langle \bar{\epsilon}\, \frac{\partial v}{\partial \mathbf{n}} \right\rangle_{E_j} = 0 \tag{39}$$

for all interface E_j, $j = 1, \ldots N_I$ and

$$\bar{\epsilon}_i \int_{\partial T_i} \frac{\partial v_i}{\partial \mathbf{n}}\, d\mathbf{y} + k \int_{T_i} v_i\, d\mathbf{x} = \bar{f}_i |T_i| \tag{40}$$

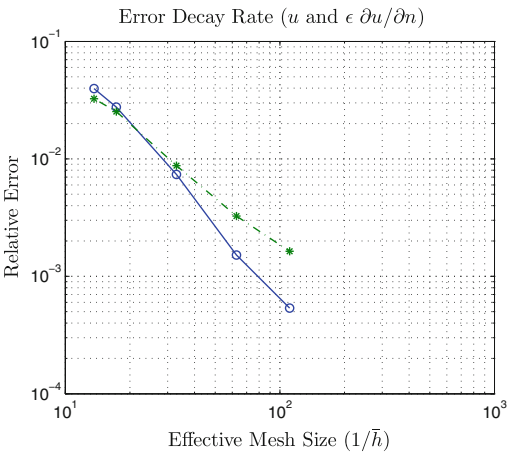

Fig. 10 Decay rates of L^2-error (*solid line*) and H^*-error (*dash-dotted line*) as a function of effective mesh size $\bar{h} = \sqrt{|\Omega|/N_T}$

for all triangles $T_i, i = 1, \ldots N_T$. Note that all of the integrals in (40) can be explicitly written with function values $\{v(M_j)\}$ on midpoints of the edges $M_j \in \partial T_i$ and the nonharmonic strength d_i. Equations (39) and (40) form a well-conditioned system of linear equations.

Figure 10 depicts the expected convergence order in the L^2-norm and in the normal derivative based H^*-norm defined in (36). Similar to the previous example, the convergence order in L^2-norm is two and H^*-norm convergence order is one and a half, which are in good agreement with the expected convergence rate.

6 Concluding remark

We introduce a numerical scheme satisfying the local conservation law and present two different numerical methods, DG type nonconforming element (NC) method and local flux matching (LF) method, depending on how we choose the unknowns. These methods work for second order elliptic problem with variable coefficients on unstructured triangular mesh and satisfy conservation law locally and globally.

Moreover, we investigate convergence behavior of iterative solver such as GMRES for the two local flux conservative methods. The (LF) method has smaller system size and much better iterative convergence than the (NC) method by eliminating constraints on function continuity. As a result, we propose the local flux matching (LF) method as a simple and efficient numerical tool compared to the native nonconforming element (NC) method. The numerical experiments validate the efficiency of the proposed method and its convergence for wide class of the second order elliptic BVPs.

Extension of the LF method for more general class of elliptic problems and higher dimensional spaces will be reported in near future. Domain decomposition idea is one of the noteworthy view points in the era of multiprocessor. Our approach like non-conforming FEM exchanges information only across each sub-domain boundary [7] so that it can be useful in parallel computing. Parallelization of the method is also one of our future research directions.

References

1. Babuska, I., Szabo, B., Katz, I.: The p-version of the finite element method. SIAM J. Numer. Anal. **18**(3), 515–545 (1981)
2. Brenner, S., Scott, R.: The Mathematical Theory of Finite Element Methods, vol. 15. Springer, Berlin (2007)
3. Brezzi, F., Fortin, M.: Mixed and Hybrid Finite Element Methods. Springer, New York (1991)
4. Chen, Z., Wu, J., Xu, Y.: Higher-order finite volume methods for elliptic boundary value problems. Advances in Computational Mathematics, vol. 37 (2012)
5. Ciarlet, P.: The Finite Element Method for Elliptic Problems, vol. 4. North Holland, Amsterdam (1978)
6. Crouzeix, M., Raviart, P.A.: Conforming and nonconforming finite element methods for solving the stationary stokes equations. i. Rev. Francaise Automat. Informat. Recherche Operationnelle Ser. Rouge **7**(3), 33–75 (1973)
7. Douglas, J. Jr., Santos, J., Sheen, D., Ye, X.: Nonconforming Galerkin methods based on quadrilateral elements for second order elliptic problems. ESAIM Math. Model. Numer. Anal. **33**(04), 747–770 (1999)
8. Eymard, R., Gallouët, T., Herbin, R.: Finite volume methods. Handbook of Numerical Analysis. North Holland, Amsterdam (2000)
9. Hermeline, F.: A finite volume method for the approximation of diffusion operators on distorted meshes. J. Comput. Phys. **160**(2), 481–499 (2000)
10. Jeon, Y., Park, E.: Nonconforming cell boundary element methods for elliptic problems on triangular mesh. Appl. Numer. Math. **58**(6), 800–814 (2008)
11. Jeon, Y., Sayas, F.: The CBEM–BEM coupling for elliptic problems. Appl. Numer. Math. **59**(10), 2374–2387 (2009)
12. Jeon, Y., Sheen, D.: Analysis of a cell boundary element method. Adv. Comput. Math. **22**(3), 201–222 (2005)
13. McGee, W., Seshaiyer, P.: Non-conforming finite element methods for nonmatching grids in three dimensions. Domain Decomposition Methods in Science and Engineering, pp. 327–334 (2005)
14. Park, C., Sheen, D.: P1-nonconforming quadrilateral finite element methods for second-order elliptic problems. SIAM J. Numer. Anal. **41**(2), 624–640 (2003)
15. Raviart, P., Thomas, J.: A mixed finite element method for 2nd order elliptic problems. Mathematical Aspects of Finite Element Methods, pp. 292–315 (1977)
16. Saad, Y., Schultz, M.: GMRES: a generalized minimal residual algorithm for solving nonsymmetric linear systems. SIAM J. Sci. Stat. Comput. **7**(3), 856–869 (1986)